Adaptive Non-singleton Interval Type-2 Fuzzy Logic Controller Design for Flexible Air-breathing Hypersonic Vehicles against Measurement Noise

Xinlong Tao[*1,2], Jianqiang Yi[*1,2], Guoliang Fan[*1,2] and Jianhong Zhang[*3]

[*1]Institute of Automation, Chinese Academy of Sciences, Beijing 100190, P. R. China
[*2]University of Chinese Academy of Sciences, Beijing 100049, P. R. China
E-mail: {taoxinlong2014, jianqiang.yi, guoliang.fan}@ia.ac.cn
[*3]Beijing Aerospace Automatic Control Institute, Beijing 100854, P. R. China
E-mail: zhangjianhong167@163.com

Abstract. In this paper, an adaptive non-singleton interval type-2 fuzzy logic controller (ANSIT2-FLC) is proposed for the flexible air-breathing hypersonic vehicle (FAHV) in order to make the velocity and altitude of the FAHV track the reference commands in a good manner when measurement noise exists in the velocity channel and altitude channel. After model linearization, a dynamic inversion controller is designed to obtain the control inputs. Then, non-singleton interval type-2 fuzzy logic system (NSIT2-FLS) is applied to deal with the measurement noise in the feedback signals as well as to approximate the uncertain terms in the dynamic inversion controller. Afterwards, adaptive laws are designed to minimize the tracking errors. Low-pass filters are further employed to filter out the high frequency noise in the output signals, while tracking differentiators (TDs) and nonlinear state observers (NSOs) are utilized to obtain the high-order derivatives of the command signals and output signals respectively. Simulations show that all the performance criteria values of ANSIT2-FLS are smaller than those of singleton IT2-FLC, which demonstrates the effectiveness of our proposed controller.

Keywords: Non-singleton Interval Type-2 Fuzzy Logic System, Dynamic Inversion Control, Flexible Air-breathing Hypersonic Vehicle, Measurement Noise

1. INTRODUCTION

Hypersonic vehicles, which can reach a speed over 5 Mach, have been investigated for more than 50 years. With the huge success of X-43A experimental vehicle [1], the researches of air-breathing hypersonic vehicles (AHVs) have been developed into a higher level. Recently, the flexible air-breathing hypersonic vehicle (FAHV) model, which takes the flexible dynamics into consideration, has been studied [2]. Compared to general AHV, the flexible dynamics will cause more uncertainties and disturbances, which may bring us more challenges in flight test. Therefore, how to deal with the uncertainties brought by the flexible dynamics and environment needs to be focused on.

Fuzzy logic system (FLS) has been widely used in handling different kinds of uncertainties. In 1975, type-2 fuzzy set (T2-FS) was first introduced by Zadeh, which is the extension of type-1 fuzzy set (T1-FS). The FLS using at least one T2-FS is called type-2 fuzzy logic system (T2-FLS) [3]. Due to the complexity of computation in general T2-FLS, almost all T2-FLSs in real world use interval type-2 fuzzy sets (IT2-FSs) instead. At the same time, the singleton fuzzifier, which considers the crisp input precise and accurate, is widely employed because of its simplicity and convenience. However, singleton FLS does not have the ability to deal with the uncertainties in inputs. Besides, measurement noise is actually unavoidable in real applications, which makes the output values we obtain imprecise and uncertain. When measurement noise is considered in close-loop system, singleton FLS may not be able to present a satisfying performance as we expect.

Non-singleton fuzzy logic system (NSFLS), which uses non-singleton fuzzifier to deal with the inputs in the beginning instead, has the advantage on handling such uncertainties [4]. The structure of non-singleton type-2 fuzzy logic system (NST2-FLS) is shown in Fig. 1. It consists of four parts: non-singleton fuzzifier, rule bases, inference and output processing, the last three of which are the same as the singleton type-2 FLS's. As non-singleton fuzzifier maps the crisp inputs into fuzzy input sets in the first step, the crisp inputs can be imprecise and uncertain, which is different from singleton FLS. Montalvo and Soto employed NSFLS in training data where the data sets were corrupted with noise [5]. Sahab and Hagras used adaptive NST2-FLS to handle the numerical uncertainties in robot navigating [6].

This paper mainly proposes an adaptive non-singleton interval type-2 fuzzy logic controller (ANSIT2-FLC) for FAHV. First, a dynamic inversion controller is designed as the basic controller to calculate the values of the control inputs. Then, for the measurement noise in the feedback signals and the uncertain terms in the dynamic inversion controller, non-singleton interval type-2 fuzzy logic system (NSIT2-FLS) is applied. Afterwards, adaptive laws are designed for improving the accuracy of approximation and minimizing the tracking errors. Low-pass filters are further employed to filter out the high frequency noise in the output signals, while tracking differentiators (TDs) and nonlinear state observers

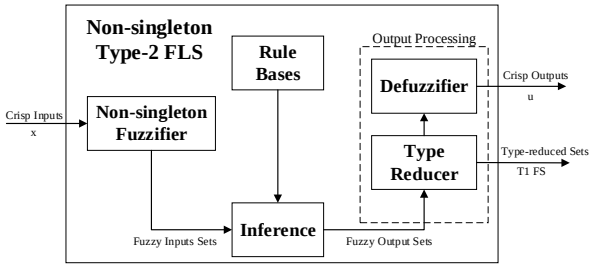

Fig. 1 The structure of NST2-FLS.

(NSOs) are utilized to obtain the high-order derivatives of the command signals and output signals respectively. Finally, comparative simulations validate the effectiveness of our proposed controller on both the velocity tracking and altitude tracking under the effect of measurement noise.

The rest of this paper is organized as follows. Section 2 states the problem which we focus on and gives some related preliminaries. Section 3 introduces the details of ANSIT2-FLC design. The simulation results are presented in Section 4, after which we draw our conclusions.

2. Problem Statement and Preliminaries

The aim of this paper is to design an ANSIT2-FLC which can make the velocity V and altitude h of the FAHV track the reference commands V_c and h_c in a good manner when measurement noise exists in the velocity channel and altitude channel. According to [7], the nonlinear longitudinal dynamic motion equations of the FAHV are given below:

$$\dot{V} = \left(T\cos\alpha - D\right)/m - g\sin\gamma \tag{1}$$

$$\dot{\gamma} = \left(L + T\sin\alpha\right)/mV - g\cos\gamma/V \tag{2}$$

$$\dot{h} = V\sin\gamma \tag{3}$$

$$\dot{\alpha} = q - \dot{\gamma} \tag{4}$$

$$\dot{q} = M_{yy}/I_{yy} \tag{5}$$

$$\ddot{\eta}_i = -2\zeta_i\omega_i\dot{\eta}_i - \omega_i^2\eta_i + N_i, \quad i = 1,2,3. \tag{6}$$

This model contains five rigid-body states $\left[V\ \gamma\ h\ \alpha\ q\right]^T$, which represent the velocity, flight path angle, altitude, angle of attack and pitch rate respectively, as well as six flexible states $\left[\eta_1\ \dot{\eta}_1\ \eta_2\ \dot{\eta}_2\ \eta_3\ \dot{\eta}_3\right]^T$, which correspond to the first three vibrational modes. The nominal operating condition is defined as the 50% fuel level condition [8], with the vehicle mass $m = 147.9\ slug/ft$ and the model frequencies $\omega_1 = 21.17 rad/s$, $\omega_2 = 53.92 rad/s$, $\omega_3 = 109.1 rad/s$. The damping ratio is a constant: $\zeta_i = 0.02$. The approximations of the lift L, drag D, thrust T, pitching moment M_{yy} and the three generalized forces N_1, N_2 and N_3 are given as follows:

$$L \approx 0.5\rho V^2 s C_L(\alpha, \boldsymbol{\delta}, \boldsymbol{\eta}) \tag{7}$$

$$D \approx 0.5\rho V^2 s C_D(\alpha, \boldsymbol{\delta}, \boldsymbol{\eta}) \tag{8}$$

$$T \approx 0.5\rho V^2 s\left[C_{T,\phi}(\alpha)\phi + C_T(\alpha) + \boldsymbol{C}_T^{\eta}\boldsymbol{\eta}\right] \tag{9}$$

$$M_{yy} \approx z_T T + 0.5\rho V^2 s\bar{c} C_M(\alpha, \boldsymbol{\delta}, \boldsymbol{\eta}) \tag{10}$$

$$N_i \approx 0.5\rho V^2 s\left[N_i^{\alpha^2}\alpha^2 + N_i^{\alpha}\alpha + N_i^{\delta_e}\delta_e + N_i^{\delta_c}\delta_c + N_i^0 + \boldsymbol{N}_i^{\eta}\boldsymbol{\eta}\right] \tag{11}$$

where ϕ stands for the throttle setting and $\boldsymbol{\delta} = \left[\delta_c, \delta_e\right]^T$, in which δ_c and δ_e represent the canard deflection and elevator deflection respectively. Besides,

$$C_{T,\phi}(\alpha) = C_T^{\phi\alpha^3}\alpha^3 + C_T^{\phi\alpha^2}\alpha^2 + C_T^{\phi\alpha}\alpha + C_T^{\phi} \tag{12}$$

$$C_T(\alpha) = C_T^3\alpha^3 + C_T^2\alpha^2 + C_T^1\alpha + C_T^0 \tag{13}$$

$$C_L(\alpha, \boldsymbol{\delta}, \boldsymbol{\eta}) = C_L^{\alpha}\alpha + C_L^{\delta_e}\delta_e + C_L^{\delta_c}\delta_c + C_L^0 + \boldsymbol{C}_L^{\eta}\boldsymbol{\eta} \tag{14}$$

$$C_D(\alpha, \boldsymbol{\delta}, \boldsymbol{\eta}) = C_D^{\alpha^2}\alpha^2 + C_D^{\alpha}\alpha + C_D^{\delta_e^2}\delta_e^2 + C_D^{\delta_e}\delta_e + C_D^{\delta_c^2}\delta_c^2 + C_D^{\delta_c}\delta_c + C_D^0 + \boldsymbol{C}_D^{\eta}\boldsymbol{\eta} \tag{15}$$

$$C_M(\alpha, \boldsymbol{\delta}, \boldsymbol{\eta}) = C_M^{\alpha^2}\alpha^2 + C_M^{\alpha}\alpha + C_M^{\delta_e}\delta_e + C_M^{\delta_c}\delta_c + C_M^0 + \boldsymbol{C}_M^{\eta}\boldsymbol{\eta} \tag{16}$$

$$\boldsymbol{C}_j^{\eta} = \left[C_j^{\eta_1}\quad 0\quad C_j^{\eta_2}\quad 0\quad C_j^{\eta_3}\quad 0\right],\ j = T, L, D, M \tag{17}$$

$$\boldsymbol{N}_i^{\eta} = \left[N_i^{\eta_1}\quad 0\quad N_i^{\eta_2}\quad 0\quad N_i^{\eta_3}\quad 0\right],\quad i = 1,2,3. \tag{18}$$

Furthermore, the canard deflection δ_c is set to be ganged with the elevator deflection δ_e [9], in the relationship of $\delta_c = k_{ec}\delta_e$ and $k_{ec} = -C_L^{\delta_e}/C_L^{\delta_c}$. The air density ρ in (7)-(11) is defined as $\rho = \rho_0\exp\left(-h/h_0\right)$, where $\rho_0 = 6.7429\times10^{-5}\ slug/ft^3$ and $h_0 = 24000\ ft$. Other coefficients in (7)-(18) can refer to [10].

In order to avoid that the decoupling matrix in feedback linearization becomes singular over the entire flight range [11], the engine dynamics can be modeled as a second-order system with the new input command ϕ_c:

$$\ddot{\phi} = -2\zeta_n\omega_n\dot{\phi} - \omega_n^2\phi + \omega_n^2\phi_c \tag{19}$$

where $\zeta_n = 0.7$ is the damping ratio of the engine and $\omega_n = 20$ is the natural frequency of the engine. At the same time, the limitations of the actuators are set as: $\delta_e, \delta_c \in \left[-20^\circ, 20^\circ\right]$, $\phi \in \left[0.05, 1.5\right]$.

3. Control Design

In order to reduce the side effects of flexible dynamics and measurement noise on the FAHV, we propose our ANSIT2-FLC. Fig. 2 shows the block diagram of the overall control system. The control inputs are selected as $\boldsymbol{u} = \left[\phi_c, \delta_e\right]^T$, while the outputs of the system are chosen as $\boldsymbol{y} = \left[V, h\right]^T$. In the rest of this section, we will introduce the design details of each part of this system.

3.1. Dynamic Inversion Controller Design

The dynamic inversion controller is designed to calculate the values of the control inputs $\boldsymbol{u} = \left[\phi_c, \delta_e\right]^T$. Based on differential geometric control theory, if the relative degree of the nonlinear system equals to the order of that system, then the nonlinear system can be completely linearized [12]. Differentiating V and h three times and four times respectively, we can obtain the

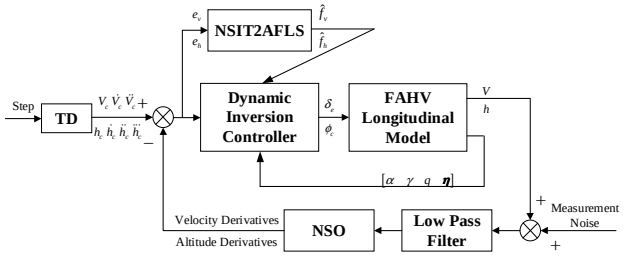

Fig. 2 The block diagram of the overall control system.

following input/output relationship:

$$\begin{bmatrix} \ddot{V} \\ h^{(4)} \end{bmatrix} = \begin{bmatrix} f_v \\ f_h \end{bmatrix} + \begin{bmatrix} b_{11} & b_{12} \\ b_{21} & b_{22} \end{bmatrix} \begin{bmatrix} \phi_c \\ \delta_e \end{bmatrix} \tag{20}$$

where

$$f_v = \left(\omega_1 \ddot{\boldsymbol{x}}_0 + \dot{\boldsymbol{x}}^T \Omega_2 \dot{\boldsymbol{x}}\right) / m \tag{21}$$

$$\begin{aligned} f_h = {} & \left(\omega_1 \ddot{\boldsymbol{x}}_0 + \dot{\boldsymbol{x}}^T \Omega_2 \dot{\boldsymbol{x}}\right) \sin\gamma / m + V\left(\pi_1 \ddot{\boldsymbol{x}}_0 + \dot{\boldsymbol{x}}^T \Pi_2 \dot{\boldsymbol{x}}\right)\cos\gamma \\ & + 3\ddot{V}\dot{\gamma}\cos\gamma - 3\dot{V}\dot{\gamma}^2 \sin\gamma + 3\dot{V}\ddot{\gamma}\cos\gamma \\ & - 3V\dot{\gamma}\ddot{\gamma}\sin\gamma - V\dot{\gamma}^3\cos\gamma \end{aligned} \tag{22}$$

$$b_{11} = \frac{\omega_n^2}{m}\frac{\partial T}{\partial \phi}\cos\alpha \tag{23}$$

$$\begin{aligned} b_{12} = {} & \frac{\rho V^2 s\bar{c}}{2mI_{yy}}\left(C_M^{\delta_e} - \frac{C_L^{\delta_e}}{C_L^{\delta_c}}C_M^{\delta_c}\right) \\ & \left(\frac{\partial T}{\partial \alpha}\cos\alpha - T\sin\alpha - \frac{\partial D}{\partial \alpha}\right) \end{aligned} \tag{24}$$

$$b_{21} = \frac{\omega_n^2}{m}\frac{\partial T}{\partial \phi}\sin(\gamma+\alpha) \tag{25}$$

$$\begin{aligned} b_{22} = {} & \frac{\rho V^2 s\bar{c}}{2mI_{yy}}\left(C_M^{\delta_e} - \frac{C_L^{\delta_e}}{C_L^{\delta_c}}C_M^{\delta_c}\right) \\ & \left[\left(\frac{\partial T}{\partial \alpha}\cos\alpha - T\sin\alpha - \frac{\partial D}{\partial \alpha}\right)\sin\gamma \right. \\ & \left. + \left(\frac{\partial L}{\partial \alpha} + \frac{\partial T}{\partial \alpha}\sin\alpha + T\cos\alpha\right)\cos\gamma\right] \end{aligned} \tag{26}$$

in which $\boldsymbol{x} = [V\ \gamma\ \alpha\ \phi\ h]^T$ and $\ddot{\boldsymbol{x}}_0 = \left[\ddot{V}\ \ddot{\gamma}\ \ddot{\alpha}_0\ \ddot{\phi}_0\ \ddot{h}\right]^T$. Then through feedback linearization, the control inputs can be written as:

$$\boldsymbol{u} = \begin{bmatrix} \phi_c \\ \delta_e \end{bmatrix} = \begin{bmatrix} b_{11} & b_{12} \\ b_{21} & b_{22} \end{bmatrix}^{-1} \begin{bmatrix} -f_v - \sum_{i=0}^{2} k_{1i} e_v^{(i)} + \ddot{V}_c \\ -f_h - \sum_{j=0}^{3} k_{2j} e_h^{(j)} + h_c^{(4)} \end{bmatrix} \tag{27}$$

where $e_v = V - V_c$ and $e_h = h - h_c$. $k_{1i}(i = 0,1,2)$ and $k_{2j}(j = 0,1,2,3)$ are chosen as the coefficients of Hurwitz polynomials $p^3 + k_{12}p^2 + k_{11}p + k_{10}$ and $p^4 + k_{23}p^3 + k_{22}p^2 + k_{21}p + k_{20}$ respectively, which lead to the exponentially stable dynamics.

3.2. Non-singleton Interval Type-2 Fuzzy Logic System Design

Since there exist disturbances of flexible dynamics and measurement noise in real applications, it is hard to obtain the precise values of f_v and f_h in (27). As a result, f_v and f_h should be considered as uncertain terms. In the rest of this paper, we replace f_v and f_h with $\hat{f}_v$ and $\hat{f}_h$ which are uncertainty-embedded, then (27) becomes:

$$\boldsymbol{u} = \begin{bmatrix} \phi_c \\ \delta_e \end{bmatrix} = \begin{bmatrix} b_{11} & b_{12} \\ b_{21} & b_{22} \end{bmatrix}^{-1} \begin{bmatrix} -\hat{f}_v - \sum_{i=0}^{2} k_{1i} e_v^{(i)} + \ddot{V}_c \\ -\hat{f}_h - \sum_{j=0}^{3} k_{2j} e_h^{(j)} + h_c^{(4)} \end{bmatrix}. \tag{28}$$

At the same time, NSIT2-FLS is designed to reduce the influence of measurement noise and to approximate the uncertain terms mentioned above.

The NSIT2-FLS has a rule base of M rules, with the general form of:

$$\begin{aligned} R^s : {} & If\ x_1\ is\ \tilde{F}_1^s\ and\ x_2\ is\ \tilde{F}_2^s, \\ & then\ u_1\ is\ G_1^s\ and\ u_2\ is\ G_2^s \quad s = 1,2,...,M \end{aligned} \tag{29}$$

where $x_1 = e_v$, $x_2 = e_h$, $u_1 = \hat{f}_v$, and $u_2 = \hat{f}_h$. The antecedent fuzzy sets $\tilde{F}_1^s$ and $\tilde{F}_2^s$ are Gaussian IT2-FSs, whose lower membership functions (LMFs) and upper membership functions (UMFs) are:

$$\underline{\mu}_{\tilde{F}_i^s}(x_i) = \exp\left(-\left(x_i - \underline{m}_{\tilde{F}_i^s}\right)^2 \Big/ 2\underline{\sigma}_{\tilde{F}_i^s}^2\right) \tag{30}$$

$$\bar{\mu}_{\tilde{F}_i^s}(x_i) = \exp\left(-\left(x_i - \bar{m}_{\tilde{F}_i^s}\right)^2 \Big/ 2\bar{\sigma}_{\tilde{F}_i^s}^2\right), \quad i = 1,2 \tag{31}$$

respectively, which can be seen in Fig. 3, while the consequent fuzzy sets G_1^s and G_2^s are Gaussian T1-FSs, whose centroids are denoted by $\boldsymbol{\theta}_v = (\theta_v^1, \theta_v^2, ..., \theta_v^M)^T$ and $\boldsymbol{\theta}_h = (\theta_h^1, \theta_h^2, ..., \theta_h^M)^T$ respectively. Besides, Gaussian non-singleton fuzzifier is chosen, with the expression of:

$$\mu_{X_i}(x_i) = \exp\left(-\left(x_i - m_{X_i}\right)^2 \Big/ 2\sigma_{X_i}^2\right). \tag{32}$$

Then, as Fig. 4 shows, the FOU of the IT2 fired output FS $\tilde{B}_m^s$ can be expressed as follows [4, 13]:

$$\mathrm{FOU}(\tilde{B}_m^s) = \left[\underline{f}^s(\boldsymbol{x}'), \bar{f}^s(\boldsymbol{x}')\right] \star \mu_{G_m^s}(u_m), \quad m = 1,2 \tag{33}$$

$$\underline{f}^s(\boldsymbol{x}') = T_{i=1}^2\left(\sup \mu_{X_i}(x_i) \star \underline{\mu}_{\tilde{F}_i^s}(x_i)\right) \tag{34}$$

$$\bar{f}^s(\boldsymbol{x}') = T_{i=1}^2\left(\sup \mu_{X_i}(x_i) \star \bar{\mu}_{\tilde{F}_i^s}(x_i)\right) \tag{35}$$

where $\boldsymbol{x}' = [x_1', x_2']^T$ are the crisp inputs of the NSIT2-FLS and $\star$ represents a t-norm. Let

$$\underline{\mu}_{Q_i^s}(x_i) = \mu_{X_i}(x_i) \star \underline{\mu}_{\tilde{F}_i^s}(x_i) \tag{36}$$

$$\bar{\mu}_{Q_i^s}(x_i) = \mu_{X_i}(x_i) \star \bar{\mu}_{\tilde{F}_i^s}(x_i). \tag{37}$$

If we use product inference and set $m_{X_i} = x_i'$, then by maximizing (36) and (37), (34) and (35) can be rewritten in the following form:

$$\underline{f}^s(\boldsymbol{x}') = \underline{\mu}_{Q_1^s}(x_{1l,\max}^s) * \underline{\mu}_{Q_2^s}(x_{2l,\max}^s) \tag{38}$$

$$\bar{f}^s(\boldsymbol{x}') = \bar{\mu}_{Q_1^s}(x_{1r,\max}^s) * \bar{\mu}_{Q_2^s}(x_{2r,\max}^s) \tag{39}$$

where

$$x_{il,\max}^s = \left(\sigma_{X_i}^2 \underline{m}_{\tilde{F}_i^s} + \underline{\sigma}_{\tilde{F}_i^s}^2 x_i'\right) \Big/ \left(\sigma_{X_i}^2 + \underline{\sigma}_{\tilde{F}_i^s}^2\right) \tag{40}$$

$$x_{ir,\max}^s = \left(\sigma_{X_i}^2 \bar{m}_{\tilde{F}_i^s} + \bar{\sigma}_{\tilde{F}_i^s}^2 x_i'\right) \Big/ \left(\sigma_{X_i}^2 + \bar{\sigma}_{\tilde{F}_i^s}^2\right) \tag{41}$$

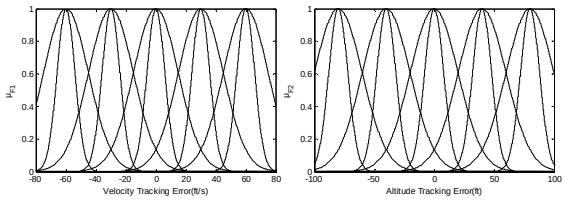

Fig. 3 The antecedent IT2-FSs $\tilde{F}_1^s$ and $\tilde{F}_2^s$.

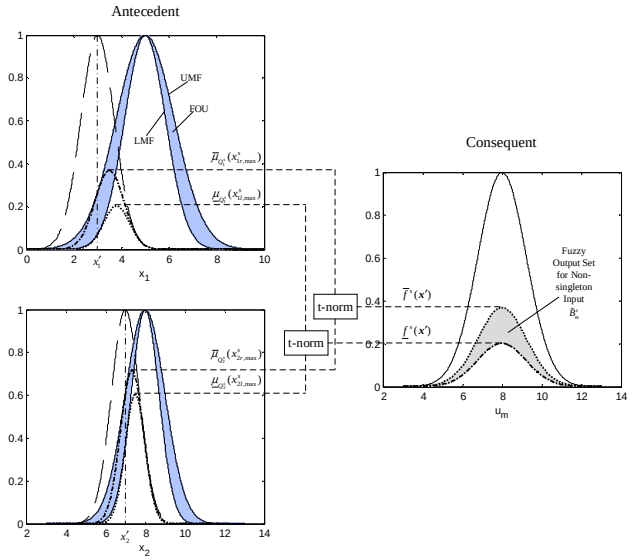

Fig. 4 The inference process of the NSIT2-FLS.

$$\underline{\mu}_{Q_i^s}(x_{il,\max}^s)=\exp\left(-\left(x_i'-\underline{m}_{\tilde{F}_i^s}\right)^2\Big/\left(2\sigma_{X_i}^2+2\underline{\sigma}_{\tilde{F}_i^s}^2\right)\right) \quad (42)$$

$$\overline{\mu}_{Q_i^s}(x_{ir,\max}^s)=\exp\left(-\left(x_i'-\overline{m}_{\tilde{F}_i^s}\right)^2\Big/\left(2\sigma_{X_i}^2+2\overline{\sigma}_{\tilde{F}_i^s}^2\right)\right). \quad (43)$$

Define the following fuzzy basic function (FBF) [4]:

$$\xi^s=w^s\Big/\sum_{s=1}^{M}w^s,\quad w^s\in\left[\underline{f}^s(\boldsymbol{x}'),\overline{f}^s(\boldsymbol{x}')\right]. \quad (44)$$

Then applying center-of-sets (COS) type reduction in the next step, we can get the type-reduced T1-FSs $u_{1\cos}$ and $u_{2\cos}$ through the Karnik-Mendel algorithm [14]:

$$\begin{aligned}u_{1\cos}&=1\Big/\left[\min\frac{\sum_{s=1}^{M}\theta_v^s w^s}{\sum_{s=1}^{M}w^s},\max\frac{\sum_{s=1}^{M}\theta_v^s w^s}{\sum_{s=1}^{M}w^s}\right]\\&=1\Big/\left[\boldsymbol{\theta}_v^T\boldsymbol{\xi}_{vl},\boldsymbol{\theta}_v^T\boldsymbol{\xi}_{vr}\right]\end{aligned} \quad (45)$$

$$\begin{aligned}u_{2\cos}&=1\Big/\left[\min\frac{\sum_{s=1}^{M}\theta_h^s w^s}{\sum_{s=1}^{M}w^s},\max\frac{\sum_{s=1}^{M}\theta_h^s w^s}{\sum_{s=1}^{M}w^s}\right]\\&=1\Big/\left[\boldsymbol{\theta}_h^T\boldsymbol{\xi}_{hl},\boldsymbol{\theta}_h^T\boldsymbol{\xi}_{hr}\right]\end{aligned} \quad (46)$$

where $\boldsymbol{\xi}_{vl}=(\xi_{vl}^1,\xi_{vl}^2,...,\xi_{vl}^M)^T$, $\boldsymbol{\xi}_{vr}=(\xi_{vr}^1,\xi_{vr}^2,...,\xi_{vr}^M)^T$, $\boldsymbol{\xi}_{hl}=(\xi_{hl}^1,\xi_{hl}^2,...,\xi_{hl}^M)^T$ and $\boldsymbol{\xi}_{hr}=(\xi_{hr}^1,\xi_{hr}^2,...,\xi_{hr}^M)^T$ are the boundary FBF vectors of (45) and (46) respectively. Finally, the crisp outputs $\hat{f}_v$ and $\hat{f}_h$ can be obtained after defuzzification

$$\hat{f}_v=\left(\boldsymbol{\theta}_v^T\boldsymbol{\xi}_{vl}+\boldsymbol{\theta}_v^T\boldsymbol{\xi}_{vr}\right)\Big/2=\boldsymbol{\theta}_v^T\left(\boldsymbol{\xi}_{vl}+\boldsymbol{\xi}_{vr}\right)\Big/2=\boldsymbol{\theta}_v^T\boldsymbol{\xi}_v \quad (47)$$

$$\hat{f}_h=\left(\boldsymbol{\theta}_h^T\boldsymbol{\xi}_{hl}+\boldsymbol{\theta}_h^T\boldsymbol{\xi}_{hr}\right)\Big/2=\boldsymbol{\theta}_h^T\left(\boldsymbol{\xi}_{hl}+\boldsymbol{\xi}_{hr}\right)\Big/2=\boldsymbol{\theta}_h^T\boldsymbol{\xi}_h. \quad (48)$$

3.3. Adaptive Laws Design

In order to improve the accuracy of approximation, we treat $\boldsymbol{\theta}_v$ and $\boldsymbol{\theta}_h$ as adaptive free parameters. Then, the adaptive laws $\dot{\boldsymbol{\theta}}_v$ and $\dot{\boldsymbol{\theta}}_h$ are required to minimize both the tracking errors and approximation errors.

According to (20) and (28), we can obtain the following dynamic equations:

$$\ddot{e}_v=-\sum_{i=0}^{2}k_{1i}e_v^{(i)}+\left(f_v-\hat{f}_v\right) \quad (49)$$

$$e_h^{(4)}=-\sum_{j=0}^{3}k_{2j}e_h^{(j)}+\left(f_h-\hat{f}_h\right). \quad (50)$$

Let

$$\boldsymbol{e}_v=(e_v,\dot{e}_v,\ddot{e}_v)^T,\quad \boldsymbol{e}_h=(e_h,\dot{e}_h,\ddot{e}_h,\dddot{e}_h)^T \quad (51)$$

$$\boldsymbol{A}_v=\begin{bmatrix}0&1&0\\0&0&1\\-k_{10}&-k_{11}&-k_{12}\end{bmatrix},\ \boldsymbol{b}_v=\begin{bmatrix}0\\0\\1\end{bmatrix} \quad (52)$$

$$\boldsymbol{A}_h=\begin{bmatrix}0&1&0&0\\0&0&1&0\\0&0&0&1\\-k_{20}&-k_{21}&-k_{22}&-k_{23}\end{bmatrix},\ \boldsymbol{b}_h=\begin{bmatrix}0\\0\\0\\1\end{bmatrix} \quad (53)$$

then (49) and (50) can be rewritten in the following form:

$$\dot{\boldsymbol{e}}_v=\boldsymbol{A}_v\boldsymbol{e}_v+\boldsymbol{b}_v\left(f_v-\hat{f}_v\right) \quad (54)$$

$$\dot{\boldsymbol{e}}_h=\boldsymbol{A}_h\boldsymbol{e}_h+\boldsymbol{b}_h\left(f_h-\hat{f}_h\right). \quad (55)$$

Assume $\boldsymbol{\theta}_v^*$ and $\boldsymbol{\theta}_h^*$ are the optimal parameter estimations:

$$\boldsymbol{\theta}_v^*=\arg\min_{\boldsymbol{\theta}_v\in\Omega_{\boldsymbol{\theta}_v}}\left(\sup\left|f_v-\hat{f}_v\right|\right),\boldsymbol{\theta}_h^*=\arg\min_{\boldsymbol{\theta}_h\in\Omega_{\boldsymbol{\theta}_h}}\left(\sup\left|f_h-\hat{f}_h\right|\right) \quad (56)$$

where

$$\Omega_{\boldsymbol{\theta}_v}=\left\{\boldsymbol{\theta}_v\in R^M\left|\theta_v^s\right|\le M_v\right\},\Omega_{\boldsymbol{\theta}_h}=\left\{\boldsymbol{\theta}_h\in R^M\left|\theta_h^s\right|\le M_h\right\} \quad (57)$$

in which M_v and M_h are positive constants. Then, the minimum approximation errors can be defined as:

$$w_v=f_v-\hat{f}_v^*,\quad w_h=f_h-\hat{f}_h^*. \quad (58)$$

With the above definitions, (54) and (55) become:

$$\begin{aligned}\dot{\boldsymbol{e}}_v&=\boldsymbol{A}_v\boldsymbol{e}_v+\boldsymbol{b}_v\left(\hat{f}_v^*-\hat{f}_v+w_v\right)\\&=\boldsymbol{A}_v\boldsymbol{e}_v+\boldsymbol{b}_v\left[\left(\boldsymbol{\theta}_v^*-\boldsymbol{\theta}_v\right)^T\boldsymbol{\xi}_v+w_v\right]\end{aligned} \quad (59)$$

$$\begin{aligned}\dot{\boldsymbol{e}}_h&=\boldsymbol{A}_h\boldsymbol{e}_h+\boldsymbol{b}_h\left(\hat{f}_h^*-\hat{f}_h+w_h\right)\\&=\boldsymbol{A}_h\boldsymbol{e}_h+\boldsymbol{b}_h\left[\left(\boldsymbol{\theta}_h^*-\boldsymbol{\theta}_h\right)^T\boldsymbol{\xi}_h+w_h\right].\end{aligned} \quad (60)$$

The Lyapunov function candidate can be chosen as follows:

$$\begin{aligned}V=&\frac{1}{2}\boldsymbol{e}_v^T\boldsymbol{P}_v\boldsymbol{e}_v+\frac{1}{2}\boldsymbol{e}_h^T\boldsymbol{P}_h\boldsymbol{e}_h+\frac{1}{2\gamma_v}\left(\boldsymbol{\theta}_v^*-\boldsymbol{\theta}_v\right)^T\left(\boldsymbol{\theta}_v^*-\boldsymbol{\theta}_v\right)\\&+\frac{1}{2\gamma_h}\left(\boldsymbol{\theta}_h^*-\boldsymbol{\theta}_h\right)^T\left(\boldsymbol{\theta}_h^*-\boldsymbol{\theta}_h\right)^T\end{aligned} \quad (61)$$

where γ_v and γ_h are positive constants, $\boldsymbol{P}_v$ and $\boldsymbol{P}_h$ are the positive definite matrices solutions of the following Lyapunov functions:

$$\boldsymbol{A}_v^T\boldsymbol{P}_v+\boldsymbol{P}_v\boldsymbol{A}_v=-\boldsymbol{Q}_v,\quad \boldsymbol{A}_h^T\boldsymbol{P}_h+\boldsymbol{P}_h\boldsymbol{A}_h=-\boldsymbol{Q}_h \quad (62)$$

respectively, in which $\boldsymbol{Q}_v$ and $\boldsymbol{Q}_h$ are appropriate positive definite square matrices. Then differentiating (61), we can get

$$\begin{aligned}\dot{V} = &-\frac{1}{2}\boldsymbol{e}_v^T\boldsymbol{Q}_v\boldsymbol{e}_v + \boldsymbol{e}_v^T\boldsymbol{P}_v\boldsymbol{b}_v w_v - \frac{1}{2}\boldsymbol{e}_h^T\boldsymbol{Q}_h\boldsymbol{e}_h + \boldsymbol{e}_h^T\boldsymbol{P}_h\boldsymbol{b}_h w_h \\ &+\frac{1}{\gamma_v}\left(\boldsymbol{\theta}_v^* - \boldsymbol{\theta}_v\right)^T\left(-\dot{\boldsymbol{\theta}}_v + \gamma_v\boldsymbol{e}_v^T\boldsymbol{P}_v\boldsymbol{b}_v\boldsymbol{\xi}_v\right) \\ &+\frac{1}{\gamma_h}\left(\boldsymbol{\theta}_h^* - \boldsymbol{\theta}_h\right)^T\left(-\dot{\boldsymbol{\theta}}_h + \gamma_h\boldsymbol{e}_h^T\boldsymbol{P}_h\boldsymbol{b}_h\boldsymbol{\xi}_h\right).\end{aligned} \tag{63}$$

As w_v and w_h should be as small as possible, the adaptive laws can be designed as:

$$\dot{\boldsymbol{\theta}}_v = \gamma_v\boldsymbol{e}_v^T\boldsymbol{P}_v\boldsymbol{b}_v\boldsymbol{\xi}_v, \quad \dot{\boldsymbol{\theta}}_h = \gamma_h\boldsymbol{e}_h^T\boldsymbol{P}_h\boldsymbol{b}_h\boldsymbol{\xi}_h \tag{64}$$

which can make $\dot{V} < 0$, leading to the close-loop stability of the system.

3.4. Low-pass Filter, Tracking Differentiator and Nonlinear State Observer Design

Besides the design of the dynamic inversion controller and ANSIT2-FLC, this paper also uses TDs and NSOs to obtain the high-order derivatives of V_c, h_c and V, h respectively which are needed in (28). Because the FAHV model is highly sensitive to measurement noise, we further use low-pass filters to filter out the high frequency signals in the velocity channel and altitude channel first.

3.4.1. Low-pass Filter Design

The transfer functions of the low-pass filters are chosen as:

$$H_v(s) = 1/(1+T_v s), \quad H_h(s) = 1/(1+T_h s). \tag{65}$$

3.4.2. Tracking Differentiator Design

TD is applied not only to form an arranged transition process but also to obtain the high-order derivatives of the command signals. (66) and (67) show the details of the discrete TD algorithms in the velocity channel and altitude channel respectively [15, 16]:

$$\begin{cases} fs_1(N) = -\lambda_v(\lambda_v(\lambda_v(V_c(N) - V_r) + 3\dot{V}_c(N)) \\ \qquad + 3\ddot{V}_c(N)) \\ V_c(N+1) = V_c(N) + \tau * \dot{V}_c(N) \\ \dot{V}_c(N+1) = \dot{V}_c(N) + \tau * \ddot{V}_c(N) \\ \ddot{V}_c(N+1) = \ddot{V}_c(N) + \tau * fs_1(N) \end{cases} \tag{66}$$

$$\begin{cases} fs_2(N) = -\lambda_h(\lambda_h(\lambda_h(\lambda_h(h_c(N) - h_r) + 4\dot{h}_c(N)) \\ \qquad + 6\ddot{h}_c(N)) + 4\dddot{h}_c(N)) \\ h_c(N+1) = h_c(N) + \tau * \dot{h}_c(N) \\ \dot{h}_c(N+1) = \dot{h}_c(N) + \tau * \ddot{h}_c(N) \\ \ddot{h}_c(N+1) = \ddot{h}_c(N) + \tau * \dddot{h}_c(N) \\ \dddot{h}_c(N+1) = \dddot{h}_c(N) + \tau * fs_2(N) \end{cases} \tag{67}$$

where N is the number of iteration, λ_v and λ_h are the "velocity factors" which are related with the speed of the arranged transition process, and τ is the time step.

3.4.3. Nonlinear State Observer Design

We use NSO to estimate the real flight states of the FAHV, especially the high-order derivatives of the outputs which are hard to measure directly. (68) and (69) show the details of the discrete NSO algorithms in the velocity channel and altitude channel respectively [15, 16]:

$$\begin{cases} e_1 = q_{11}(N) - V \\ q_{11}(N+1) = q_{11}(N) + \tau * (q_{12}(N) - \mu_{11} * e_1) \\ q_{12}(N+1) = q_{12}(N) + \tau * (q_{13}(N) \\ \qquad - \mu_{12} * fal(e_1, 0.5, \tau)) \\ q_{13}(N+1) = q_{13}(N) + \tau * (-\mu_{13} * fal(e_1, 0.25, \tau) \\ \qquad + v_{adjust} * U_1) \end{cases} \tag{68}$$

$$\begin{cases} e_2 = q_{21}(N) - h \\ q_{21}(N+1) = q_{21}(N) + \tau * (q_{22}(N) - \mu_{21} * e_2) \\ q_{22}(N+1) = q_{22}(N) + \tau * (q_{23}(N) \\ \qquad - \mu_{22} * fal(e_2, 0.5, \tau)) \\ q_{23}(N+1) = q_{23}(N) + \tau * (q_{24}(N) \\ \qquad - \mu_{23} * fal(e_2, 0.25, \tau)) \\ q_{24}(N+1) = q_{24}(N) + \tau * (-\mu_{24} * fal(e_2, 0.125, \tau) \\ \qquad + h_{adjust} * U_2) \end{cases} \tag{69}$$

where N is the number of iteration, q_{11}, q_{12}, q_{13} and $q_{21}, q_{22}, q_{23}, q_{24}$ denote $V, \dot{V}, \ddot{V}$ and $h, \dot{h}, \ddot{h}, \dddot{h}$ respectively, $\mu_{11}, \mu_{12}, \mu_{13}$ and $\mu_{21}, \mu_{22}, \mu_{23}, \mu_{24}$ are the "tracking coefficients" which are related with the observer performance, $U_1 = b_{11}\phi_c + b_{12}\delta_e$, $U_2 = b_{21}\phi_c + b_{22}\delta_e$, and τ is the time step.

4. SIMULATION

To validate the effectiveness of our proposed ANSIT2-FLC, the simulations take adaptive singleton IT2-FLC as a comparison. The simulations start with the initial condition of $V_0 = 7846.4\,ft/s$, $\gamma_0 = 0\,rad$, $h_0 = 85000\,ft$, $\alpha_0 = 0.0219\,rad$, $q_0 = 0\,rad/s$, $\eta_1 = 0.594 ft\sqrt{slug}$, $\eta_2 = -0.0976\,ft\sqrt{slug}$, $\eta_3 = -0.0335\,ft\sqrt{slug}$ and $\dot{\eta}_1 = \dot{\eta}_2 = \dot{\eta}_3 = 0\ ft\sqrt{slug}/s$. Step signals are used as the reference commands: $300\,ft/s$ in velocity channel and $4000\,ft$ in altitude channel. The parameters of the antecedent fuzzy sets $\tilde{F}_1^s$ and $\tilde{F}_2^s$ are set in Table. 1, while the initial values of the adaptive parameters $\boldsymbol{\theta}_v$ and $\boldsymbol{\theta}_h$ are chosen randomly. Other parameters in ANSIT2-FLC are set as $k_{10} = 0.0100$, $k_{11} = 3.9495$, $k_{12} = 14.4401$, $k_{20} = 292.4550$, $k_{21} = 934.2200$, $k_{22} = 312.7000$, $k_{23} = 191.2500$, $Q_1 = 5I$, $Q_2 = 60000I$, $\gamma_1 = 2$, $\gamma_2 = 2$, $\sigma_{x_1} = 6$, $\sigma_{x_2} = 10$. The coefficients of the low-pass filters, TDs and NSOs are given in Table. 2.

When the measurement noise is set as $20\,db$ white Gaussian noise (WGN) in the velocity channel and

Table. 1 The parameters of $\tilde{F}_1^s$ and $\tilde{F}_2^s$.

	$\tilde{F}_1^s$				$\tilde{F}_2^s$			
	$\underline{m}_{\tilde{F}_i^s}$	$\underline{\sigma}_{\tilde{F}_i^s}$	$\bar{m}_{\tilde{F}_i^s}$	$\bar{\sigma}_{\tilde{F}_i^s}$	$\underline{m}_{\tilde{F}_i^s}$	$\underline{\sigma}_{\tilde{F}_i^s}$	$\bar{m}_{\tilde{F}_i^s}$	$\bar{\sigma}_{\tilde{F}_i^s}$
NB	-60	6	-60	15	-80	8	-80	20
NS	-30	6	-30	15	-40	8	-40	20
ZO	0	6	0	15	0	8	0	20
PS	30	6	30	15	40	8	40	20
PB	60	6	60	15	80	8	80	20

Table. 2 The coefficients of the low-pass filters, TDs and NSOs.

Parameters	Value	Parameters	Value
T_v	0.5	T_h	0.5
$\lambda_{v,h}$	0.35,0.2	τ	0.01
$\mu_{11,12,13}$	150,500,3500	$\mu_{21,22,23,24}$	180,300,1500,2200

altitude channel, the results can be seen in Fig. 5 and Fig. 6. As Fig. 5 shows, ANSIT2-FLC has a smaller overshoot and a smoother steady-state response than the adaptive singleton IT2-FLC in both the velocity channel and altitude channel due to the effect of the non-singleton fuzzifier on the uncertain controller inputs. Furthermore, according to Fig. 6, the elevator deflection of ANSIT2-FLC vibrates smaller under the effect of measurement noise, which means the proposed controller outperforms its comparison in this case.

In addition, we apply integral of square error (ISE), integral of the absolute value of the error (IAE) and integral of the time multiplied by the absolute value of the error (ITAE) for evaluating the performances of the two controllers. The values of the three performance criteria of the velocity channel and altitude channel are shown in Table. 3 and Table. 4 respectively. From the tables we can see that all the performance criteria values of ANSIT2-FLS are smaller than those of singleton IT2-FLC, which demonstrates the effectiveness of our proposed controller. Besides, in the velocity channel, the ISE of our proposed controller is 29.0% lower than that of singleton IT2-FLC, while in the altitude channel the ISE of ANSIT2-FLC is 3.2% lower than its comparison, which means that non-singleton fuzzifier performs better in reducing the side effect of measurement noise on the velocity tracking.

5. CONCLUSIONS

This paper presents an adaptive non-singleton interval type-2 fuzzy logic controller design for flexible air-breathing hypersonic vehicles against measurement noise. Compared with singleton IT2-FLS, NSIT2-FLS has the advantage on dealing with the uncertainties in input signals. Low-pass filters are employed to filter out the high frequency noise in the feedback signals, while non-singleton fuzzifiers are utilized to reduce the side effect of the low frequency noise on the velocity tracking and altitude tracking. Through Lyapunov approach, the adaptive free parameters can be tuned by adaptive laws in real time and the accuracy of approximation can be

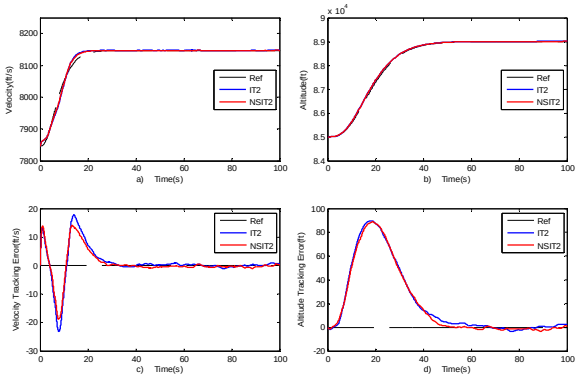

Fig. 5 Velocity and altitude responses with 20 *db* WGN.

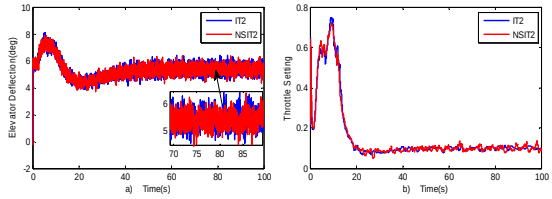

Fig. 6 Control inputs with 20 *db* WGN.

Table. 3 Performance criteria of the velocity channel.

Controller	ISE	IAE	ITAE
singleton IT2	3390.7	280.11	4763.1
ANSIT2-FLC	2407.4	240.91	4375.8

Table. 4 Performance criteria of the altitude channel.

Controller	ISE	IAE	ITAE
singleton IT2	1.311×10^5	2111.2	5.059×10^4
ANSIT2-FLC	1.269×10^5	2029.8	4.730×10^4

improved. Applying TDs and NSOs, we can obtain the high-order derivatives of the outputs which are hard to measure directly. Finally, the comparative simulations have shown that all the performance criteria values of ANSIT2-FLC are smaller than those of singleton IT2-FLC, which demonstrates the effectiveness of our proposed controller on both the velocity tracking and altitude tracking under the effect of measurement noise. This is the first attempt to consider the measurement noise in FAHV tracking problems. How to further reduce the effect of the measurement noise on the actuators will be investigated in our next research.

Acknowledgements

This work is supported by NNSFC No. 61421004, No. 61273149 and NDBSR No. B1320133020. The authors also gratefully acknowledge the helpful comments and suggestions of the reviewers, which have improved the presentation.

REFERENCES:

[1] P. V. Tartabini, D. M. Bose, M. N. Thornblom, J. Lien, and J. G. Martin, "Mach 10 stage separation analysis for the X43-A," 44th AIAA Aerospace Sciences Meeting and Exhibit, Reno, Nevada, 2006.

[2] M. A. Bolender and D. B. Doman, "Nonlinear longitudinal dynamical model of an air-breathing hypersonic vehicle," Journal of Spacecraft and Rockets, vol. 44, pp. 374-387, 2007.

[3] J. M. Mendel, "Type-2 fuzzy sets and systems: an overview," IEEE Computational Intelligence Magazine, vol. 2, pp. 20-29, 2007.

[4] G. C. Mouzouris and J. M. Mendel, "Nonsingleton fuzzy logic systems: theory and application," IEEE Transactions on Fuzzy Systems, vol. 5, pp. 56-71, 1997.

[5] G. Montalvo and R. Soto, "Methodology for handling uncertainty by using interval type-2 Fuzzy Logic Systems," MICAI 2004: Advances in Artificial Intelligence, pp. 536-545, 2004.

[6] N. Sahab and H. Hagras, "Adaptive non-singleton type-2 fuzzy logic systems: a way forward for handling numerical uncertainties in real world applications," International Journal of Computers Communications & Control, vol. 6, pp. 503-529, 2011.

[7] L. Fiorentini, A. Serrani, M. A. Bolender, and D. B. Doman, "Nonlinear robust adaptive control of flexible air-breathing hypersonic vehicles," Journal of Guidance, Control, and Dynamics, vol. 32, pp. 402-417, 2009.

[8] D. Sigthorsson, P. Jankovsky, A. Serrani, S. Yurkovich, M. Bolender, and D. B. Doman, "Robust linear output feedback control of an airbreathing hypersonic vehicle," Journal of Guidance, Control, and Dynamics, vol. 31, pp. 1052-1066, 2008.

[9] M. A. Bolender and D. B. Doman, "Flight path angle dynamics of air-breathing hypersonic vehicles," AIAA Paper 2006-6692, 2006.

[10] L. Fiorentini, "Nonlinear adaptive controller design for air-breathing hypersonic vehicles," Ph.D dissertation, Electrical and Computer Engineering Department, The Ohio State University, 2010.

[11] J. T. Parker, A. Serrani, S. Yurkovich, M. A. Bolender, and D. B. Doman, "Control-oriented modeling of an air-breathing hypersonic vehicle," Journal of Guidance, Control, and Dynamics, vol. 30, pp. 856-869, 2007.

[12] H. Xu, M. D. Mirmirani, and P. A. Ioannou, "Adaptive sliding mode control design for a hypersonic flight vehicle," Journal of Guidance, Control, and Dynamics, vol. 27, pp. 829-838, 2004.

[13] J. M. Mendel, R. I. John, and F. Liu, "Interval type-2 fuzzy logic systems made simple," IEEE Transactions on Fuzzy Systems, vol. 14, pp. 808-821, 2006.

[14] J. M. Mendel, "On KM algorithms for solving type-2 fuzzy set problems," IEEE Transactions on Fuzzy Systems, vol. 21, pp. 426-446, 2013.

[15] J. Han, Active disturbance rejection control technique-the technique for estimating and compensating the uncertainties, National Defense Industry Press Beijing, China (in Chinese), 2008.

[16] J. Gao, R. Yuan, J. Yi, and C. Li, "Adaptive interval type-2 fuzzy sliding mode controller design for flexible air-breathing hypersonic vehicles," 2015 IEEE International Conference on Fuzzy Systems (FUZZ-IEEE), 2015.